Kapal: Jurnal Ilmu Pengetahuan dan Teknologi Kelautan
(Kapal: Journal of Marine Science and Technology)
journal homepage : http://ejournal.undip.ac.id/index.php/kapal
2301-9069 (e)
1829-8370 (p)

CFD-Based Analysis of Wingsail Shape and Placement on a Fishing Vessel in Southern Bali Waters

Happy Nabila Sukmawardana[1)*], Endah Suwarni[2)], Dian Purnamasari[2)], Mohammad Ridwan Utina[2)], Rina[2)], Nanang Setiyobudi[2)], Wiwin Sulistyawati[1)]

[1)] Department of Naval Architecture, Pembangunan Nasional "Veteran" Jakarta University, Jakarta 12450, Indonesia
[2)] Research Center for Hydrodynamic Technology, National Research and Innovation Agency, Surabaya 60117, Indonesia
[*)] Corresponding Author: 2210313052@mahasiswa.upnvj.ac.id

Article Info

Keywords:
Aerodynamics;
Airfoil;
Wingsail;
Fishing Vessel

Article history:
Received: 11/02/2026
Last revised: 23/04/2026
Accepted: 11/05/2026
Available online: 11/05/2026
Published: 16/05/2026

DOI:
https://doi.org/10.14710/kapal.v23i1.82416

Abstract

The maritime transportation sector contributes significantly to atmospheric emissions due to its reliance on fossil fuels, underscoring the need for more energy-efficient, environmentally friendly propulsion technologies. One promising solution is Wind-Assisted Ship Propulsion (WASP), which uses wind energy as a supplemental power source for vessel propulsion. Among various WASP technologies, wingsails have attracted attention for their rigid airfoil geometry and their ability to generate aerodynamic lift efficiently. This study aims to investigate the influence of wing sail shape and placement on aerodynamic performance, to identify an effective configuration for vessel applications. Computational Fluid Dynamics (CFD) simulations are conducted using k-ω SST turbulence model. Two symmetric airfoil profiles, NACA 0012 and NACA 0015, are examined under angle of attack variations of 5°, 0°, 5°, 10°, 15°, and 20°. The wingsail is modeled in two installation configurations: midship and a combined midship-aft arrangement. Simulations are performed at wind speeds of 4 m/s, 10 m/s, 13.7 m/s, and 17.2 m/s, with aerodynamic performance evaluated based on the lift and drag coefficients. Based on the results, the NACA 0015 wingsail shows more stable aerodynamic behavior than the NACA 0012, while medium wind speeds in the range of 10–13.7 m/s offer the best balance between lift and drag. In addition, the midship–aft wingsail arrangement consistently generates higher lift than the single midship configuration, making the NACA 0015 wingsail with midship–aft placement the most suitable choice for fishing vessel applications.

1. Introduction

The maritime transportation sector contributes significantly to atmospheric emissions, primarily by fossil fuels in vessel propulsion systems [1]. These emissions include carbon dioxide (CO2), nitrogen oxides (NO2), sulfur oxides (SOX), and other particulate matter, which directly affect air quality and contribute to climate change. The continuous growth of global shipping activities has led to a significant increase in emissions from the maritime sector. This trend has raised concerns over its environmental impact, particularly on air quality and climate change. In response, international regulations such as MARPOL Annex VI have been introduced to limit vessel exhaust emissions [2]. This situation necessitates the development of technical solutions to reduce emissions and improve vessel energy efficiency [3]. One promising approach is the utilization of wind energy through Wind-Assisted Ship Propulsion (WASP) systems.

Wind-Assisted Ship Propulsion (WASP) is a supplementary propulsion concept for vessels that utilize wind energy to generate propulsive force, thereby reducing the workload of the main engine and overall fuel consumption [4]. The WASP system operates by converting the kinetic energy of the wind into aerodynamic forces that assist vessel motion and has been developed in various forms, including conventional sails, rotor sails, kite sails, and wingsails [5]. Among these WASP technologies, wingsails have attracted considerable attention. Their rigid, airfoil-shaped structure enables higher aerodynamic efficiency in generating lift compared to traditional sails. These characteristics make wingsails a promising solution for improving energy efficiency and reducing exhaust emissions from vessels [6].

A double flap wingsail capable of achieving a maximum lift coefficient of 1.68 has been developed, significantly improving propulsion efficiency and reducing greenhouse gas emissions [7]. Meanwhile, previous studies have shown that NACA 0015 airfoils can increase thrust through sail angle optimization [8]. In addition, hard wingsail-assisted propulsion has been comprehensively evaluated on a bulk carrier, integrating aerodynamic, stability, structural, and power analyses. The results show that rigid wingsails can significantly improve energy efficiency while reducing engine power demand without compromising safety [9]. The NACA 0012 airfoil is a symmetric profile that has been widely studied for its aerodynamic

characteristics, particularly in relation to lift and drag behavior across different angles of attack and flow conditions [10][11]. Experimental and numerical studies have consistently shown that the lift coefficient increases with the angle of attack until reaching a stall condition. In contrast, the drag coefficient gradually increases due to flow separation effects [12].

Furthermore, an innovative articulating rigid wingsail with active camber control has been developed, supported by CFD analysis and wind tunnel experiments. The results indicate a significant increase in lift coefficient compared to conventional rigid airfoils, highlighting its strong potential for improving vessel energy efficiency in wind-assisted ship propulsion systems [13]. Furthermore, a towing tank experiment on a fishing vessel fitted with a NACA 0015 wingsail installed at the midship position was conducted. The results showed that wind-assisted propulsion can effectively improve vessel performance and support more efficient operation, particularly for small-scale fishing vessels [14]. Finally, a CFD-based symmetric dual rigid wingsail design has been proposed, achieving up to a 37% increase in lift coefficient and improved thrust efficiency compared to conventional flexible designs [15].

Although previous studies have extensively investigated the aerodynamic performance of wingsails and their application in wind-assisted ship propulsion systems, most of this research has focused on large commercial vessels [16] or general aerodynamic optimization. Several studies have examined different airfoil shapes, such as the NACA series, demonstrating their effectiveness in improving lift and propulsion efficiency. Previous studies have also reported that certain wingsail configurations can significantly increase the lift coefficient [17], particularly at optimized angles of attack and airfoil geometries, highlighting the strong influence of aerodynamic parameters on performance. However, limited attention has been given to the application of wingsails on small-scale fishing vessels, particularly regarding placement and airfoil selection under realistic operational conditions. Furthermore, existing studies commonly install wingsails on the starboard and port sides of vessels [18], while the influence of alternative configurations, such as midship and midship-aft placements, remains insufficiently explored. This aspect is especially critical for fishing vessels, which have limited deck space and are highly sensitive to weight distribution and stability, making wingsail placement an important yet unresolved design consideration.

The objective of this study is to determine the optimal wingsail placement configuration for fishing vessels and to evaluate the influence of airfoil shape on aerodynamic performance. To achieve this, the study provides a detailed analysis of wingsail performance by systematically comparing midship and midship-aft placement configurations. In addition, it examines the effects of airfoil type, specifically the NACA 0012 and NACA 0015 profiles, as well as variations in angle of attack and wind speed on lift and drag characteristics. The aerodynamic performance of each configuration is assessed through the evaluation of lift and drag coefficients. All simulations are carried out using Computational Fluid Dynamics to model the airflow around the wingsail under realistic environmental conditions in the Southern Bali waters.

This study is particularly relevant for small-scale fishing vessels, where practical limitations such as restricted deck space and sensitivity to weight distribution make the selection of wingsail configuration a critical design factor. Therefore, this study contributes to the existing body of knowledge by offering a comprehensive evaluation of wingsail placement and airfoil performance specifically for fishing vessels, which remain relatively underexplored in previous studies.

2. Method

2.1. Wingsail Principle

Wind-Assisted Ship Propulsion (WASP) is a technology that harnesses wind energy to generate aerodynamic forces that increase a vessel's thrust. This technology aims to reduce fossil fuel consumption and mitigate greenhouse gas emissions produced by the main propulsion system [19]. Rather than replacing the primary propulsion, WASP functions as a supplementary system that operates parallel to enhance the overall efficiency of the vessel's propulsion.

One of the key applications of WASP technology is wingsails, also known as hard sails. Wing sails operate similarly to conventional soft sails but offer the advantage of actively adjustable curvature. This adaptability enables wingsails to achieve a higher lift-to-drag ratio, thereby enhancing the vessel's overall aerodynamic efficiency and controllability. They are typically constructed from metal, plastic, or composite fabric designed to ensure structural integrity while minimizing weight [5].

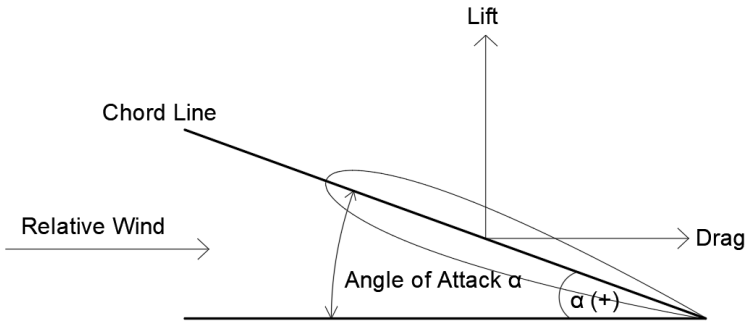

Figure 1. Airfoil schematic

Figure 1 is a schematic diagram illustrating the geometry of the wingsail, the primary element that generates aerodynamic force and contributes to vessel propulsion. When the wingsail interacts with the wind flow at a certain speed, aerodynamic forces in the form of lift and drag will be generated, where the drag force acts in the same direction as the wind

flow. Meanwhile, the lift force acts perpendicular to the flow direction. In a wingsail system, these forces can be resolved into thrust components that act parallel to the vessel's direction of motion. At the same time, lateral forces are generated, which may influence the vessel's stability. The lift force on the wingsail is generated by the difference in pressure distribution between the two sides of the wingsail surface due to differences in the speed of the airflow around it. The curved airfoil profile directs the airflow so that there are an acceleration of flow and a decrease in pressure on one side of the wingsail surface, which ultimately increases the lift force generated and allows it to be used as an auxiliary propulsion force on the vessel[20].

2.2. Aerodynamic Force

To analyze the aerodynamic characteristics of wingsails, several key parameters are considered, including lift force and drag force. The aerodynamic performance is evaluated using a theoretical approach based on established formulations for lift and drag coefficients [7]. The equations used in this study are presented below:

Lift coefficient of the sail

$$C_L = \frac{F_L}{(0.5\ \rho_\alpha\ {V_r}^2 S)} \quad (1)$$

Drag coefficient of the sail

$$C_D = \frac{F_D}{(0.5\ \rho_\alpha\ {V_r}^2 S)} \quad (2)$$

These equations denote the lift and drag coefficients of the wingsail, CL and CD, respectively. The symbols FL and FD represent the lift and drag forces acting on the wingsail. The angle of attack is expressed by α, V represents the wind velocity, S denotes the sail area, and ρ refers to the air density.

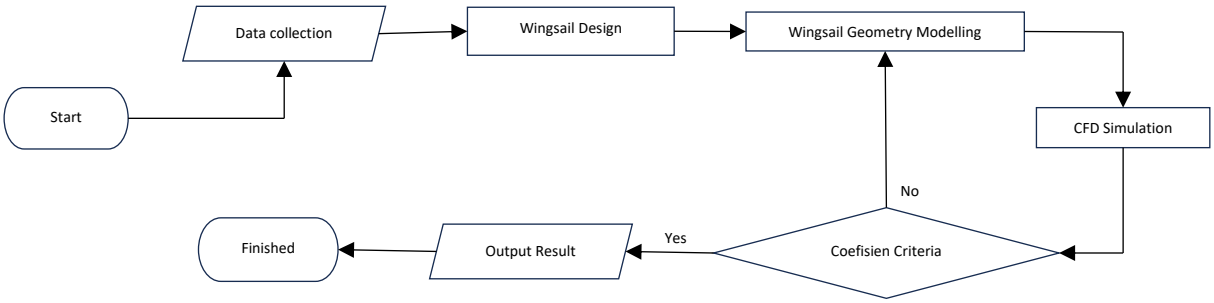

Figure 2. Methodology framework

The flowchart in Figure 2 outlines the methodology used in this study to evaluate the aerodynamic performance of various wing-sail configurations. The process begins with the data collection stage, which includes vessel specifications, operational environmental conditions, and relevant references for wingsail design, followed by the wingsail design stage, where variations in airfoil shape, angle of attack, and mounting position are defined based on literature and technical considerations. The next stage involves wingsail geometry modeling and CFD simulation to analyze the aerodynamic behavior of each configuration. To evaluate the simulation results, a coefficient-based criterion is applied, focusing on the lift coefficient (CL) and drag coefficient (CD), where the results are considered acceptable when the lift coefficient exceeds approximately -0.7. In contrast, the drag coefficient remains below 0.6. A "yes" decision indicates that the configuration satisfies the expected aerodynamic performance, whereas a "no" decision suggests that further refinement is required. This process is carried out iteratively until an optimal configuration is obtained, after which the final results are analyzed.

2.3. Vessel Data

The object of this study is a long line tuna fishing vessel with a capacity of 256 GT. The general arrangement and principal dimensions of the vessel are illustrated through the sheer plan shown in Figure 3, which serves as the reference geometry for the wingsail installation analysis. The sheer plan provides an overview of the vessel's profile and layout, serving as the basis for determining the wingsail placement configuration in the present study. The main dimension of the 265 GT long line fishing vessel used in this study is presented in Table 1.

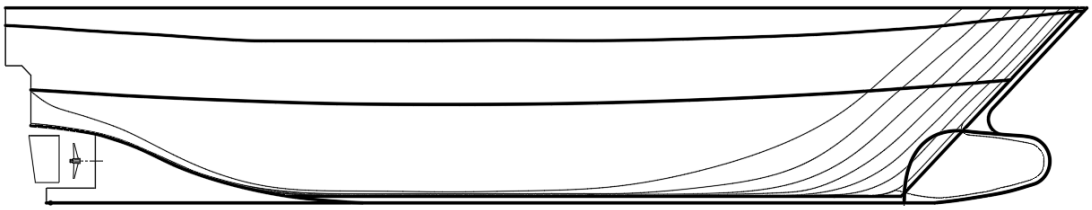

Figure 3. Sheer plan of object vessel

Table 1. The main dimension of the vessel

Dimension	Notation	Value
Length Over All (m)	L_{OA}	33.500
Length of Water Line (m)	L_{WL}	29.667
Length Between Perpendiculars (m)	L_{PP}	29.054
Breadth (m)	B	7.950
Height (m)	H	6.026
Draft (m)	T	2.950
Displacement (ton)	Δ	487.23

2.4. Wingsails Data

The wingsail geometry used in this study is based on the symmetric NACA 0012 and NACA 0015 airfoil profiles. The NACA 0012 airfoil is shown in Figure 4, while the NACA 0015 airfoil is presented in Figure 5. The wingsail is modelled as a three-dimensional structure with a constant NACA airfoil cross-section extruded vertically along the wingsail height, forming a rigid wingsail geometry as illustrated in Figure 6.

Figure 4. Airfoil of NACA 0012

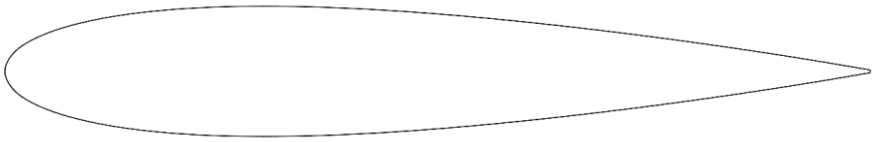

Figure 5. The Airfoil of NACA 0015

The NACA 0012 and NACA 0015 airfoils used in this study are symmetric profiles with zero camber. The maximum thickness is located at 30% of the chord length, corresponding to thickness ratios of 12% and 15%, respectively [21]. These airfoils were selected due to their symmetrical geometry and stable aerodynamic characteristics, which enable consistent evaluation of lift and drag performance without camber-induced bias. Table 2 shows the geometric dimensions of the wingsail used in this study. These dimensions are designed to ensure compatibility between the wingsail and the 265 GT fishing vessel subject to this study.

Table 2. The Dimension of The Wingsail

Dimension	Value
Height of Wingsail (m)	7.3
Height of Mast (m)	2.7
Total Height (m)	10
Chord Length (m)	2.85

The selected wingsail dimensions were determined based on proportional scaling relative to the vessel size to ensure both aerodynamic effectiveness and structural feasibility. In addition, the aspect ratio of the wingsail, defined as the ratio of height to chord length, was considered in the design process. The resulting aspect ratio of approximately 2.56 represents a moderate configuration, providing a compromise between aerodynamic performance and structural stability. Furthermore, the selected dimensions were referenced from a fishing vessel of similar scale, namely the Balueiro Segundo, which utilizes a suction sail system [22]. This comparison was adopted due to the similarity in vessel size, allowing the wingsail dimensions in this study to be defined within a realistic and practical range.

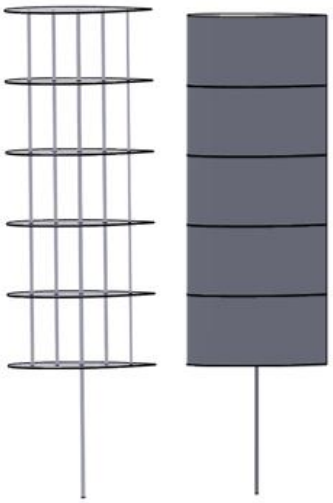

Figure 6. Wingsail with NACA 0012 and NACA 0015

This study investigates the influence of wingsail configuration on the aerodynamic performance of a fishing vessel using Computational Fluid Dynamics (CFD). The simulations are carried out in ANSYS Fluent to evaluate the effects of airfoil type, angle of attack, and wingsail placement on lift and drag characteristics. Three primary parameters were considered in the analysis: the wingsail airfoil profile, the angle of attack, and the longitudinal placement of the wingsail relative to the vessel structure.

For the airfoil configuration, two symmetric profiles, NACA 0012 and NACA 0015, were selected. These airfoils are widely applied in aerodynamic studies due to their stable characteristics and their capability to generate appreciable lift over a broad range of operating angles.

The angle of attack was defined as the angle between the incoming wind direction and the chord line of the wingsail. Variations of 5°, 0°, 5°, 10°, 15°, and 20° were evaluated to assess their effects on aerodynamic forces, including lift and drag, as well as the resulting contribution to vessel propulsion, as summarized in Table 3. The selected angle of attack range represents typical operating conditions of wingsail systems, encompassing both pre-stall and near-stall regimes. This range enables a comprehensive evaluation of aerodynamic performance, including lift generation and flow separation under varying wind conditions.

In addition, the effect of wingsail placement was examined by considering two mounting configurations: a midship arrangement (Figure 7) and a combined midship–aft arrangement (Figure 8). For the combined configuration, two wingsails were installed along the vessel centerline, with longitudinal spacing of 14.7 m between the midship and aft wingsails. These configurations were selected to evaluate potential flow interactions between the wingsail and the vessel structure, as well as wake interference effects that may influence overall aerodynamic performance. The purpose of this analysis is to evaluate the aerodynamic performance of wingsail airfoil profiles applied to fishing vessels, based on the assessment of lift coefficient and drag coefficient at wind speeds 4 m/s, 10 m/s, 13.7 m/s, and 17.2 m/s.

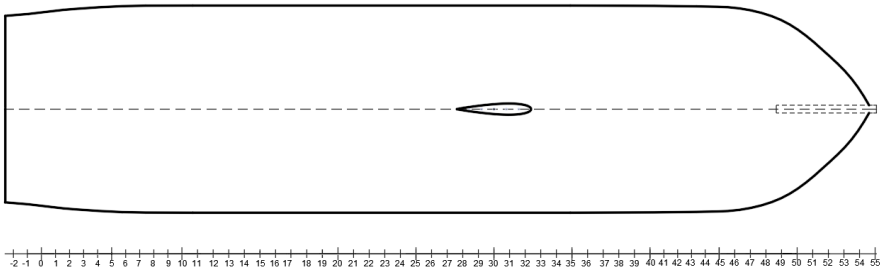

Figure 6. Position of The Wingsail in Midship

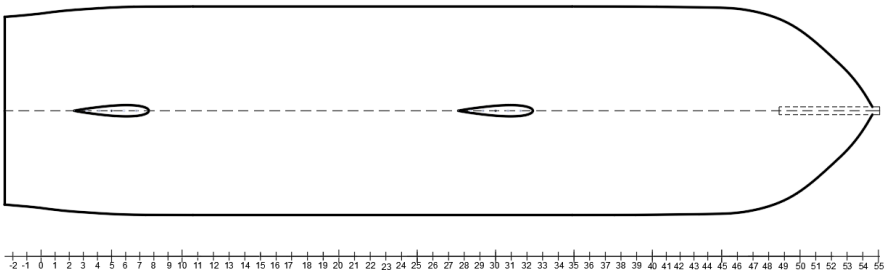

Figure 7. Position of The Wingsail in Combined Midship-aft

Table 3. Wingsail CFD analysis matrix

Configuration	Airfoil Type	Wingsail Placement	Angle of Attack
W1	NACA 0012	Midship	-5
			0
			5
			10
			15
			20
W2	NACA 0015		-5
			0
			5
			10
			15
			20
W3	NACA 0012	Midship-Aft	-5
			0
			5
			10
			15
			20
W4	NACA 0015		-5
			0
			5
			10
			15
			20

2.5. Numerical Set-up

The computational domain was defined as a three-dimensional external flow region representing the airflow around the vessel and the wingsail, as shown in Figure 9. A rectangular domain was used, with the wingsail positioned at its center to ensure a balanced flow distribution. Table 4 explained that the inlet and outlet boundaries were located at distances of 9.5 c and 10.5 c from the wingsail, respectively, where c is chord length. It results in a total domain length of 20 c in the flow direction, where c denotes the wingsail chord length. The upper and lower boundaries were placed at 5c from the wingsail to minimize boundary interference effect, particularly at higher angles of attack. The domain dimensions were defined based on standard practices in external aerodynamic CFD simulations and supported by previous studies [9]. The selected domain size ensures sufficient distance between the boundaries and the wingsail, thereby minimizing blockage effects and boundary interference. In addition, a symmetry plan was applied to the computational domain to reduce computational cost and facilitate boundary layer development and analysis on the wingsail surface.

Table 4. Computational Domain Boundary Conditions

Boundary	Distance (m)	Description
Inlet	9.5c	Distance from wingsail to inlet
Outlet	10.5c	Distance from wingsail to outlet
Top	5c	Distance from wingsail to top boundary
Bottom	5c	Distance from wingsail to bottom boundary
Side	20c	Distance from wingsail to side boundaries

Figure 10 shows the computational domain with two wingsails placed in the midship and aft positions, providing a comparison of the aerodynamic effects between the single and dual wingsail configurations.

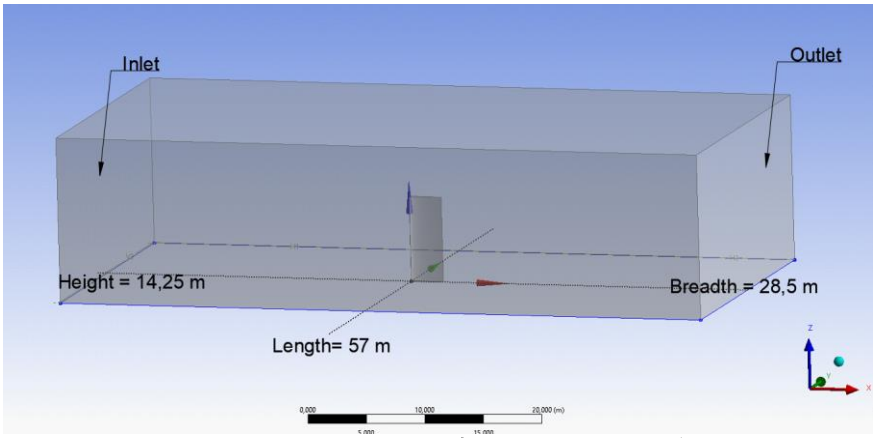

Figure 8. Domain in configuration 1 wingsail

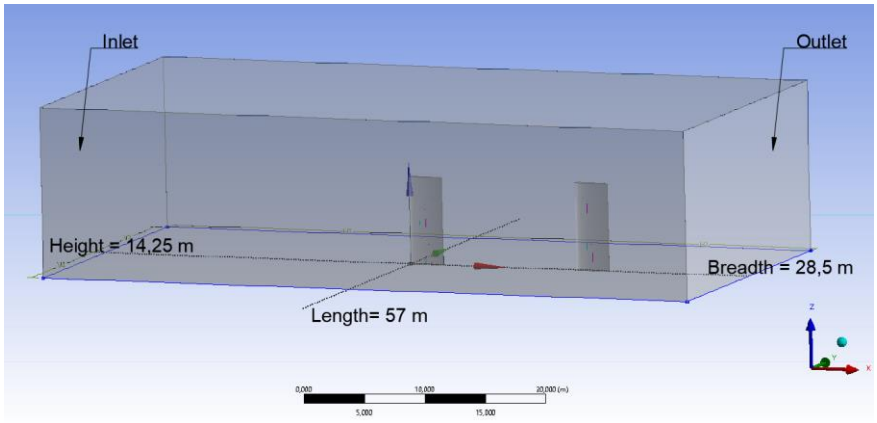

Figure 9. Domain in configuration 2 wingsail

The computational domain was discretized using a three-dimensional unstructured mesh generated with ANSYS meshing. A finer mesh resolution was applied in the vicinity of the wingsail surfaces to capture flow characteristics and aerodynamic forces accurately. A coarser mesh was used in regions farther away from the body to improve computational efficiency. The mesh configuration for the single wingsail arrangement is shown in Figure 11. The detailed mesh distribution on the wingsail surface is illustrated in Figure 12. The final mesh consisted of approximately 700,000 cells. To ensure the accuracy of the simulation results, mesh density was varied, with the number of elements ranging from approximately 431,954 to 1,192,745 cells. The lift coefficient exhibited notable changes from coarse to medium meshes, but it began to stabilize at approximately 700,000 cells.

In contrast, the drag coefficient showed only minor variations across the different mesh levels. Based on these findings, a mesh density of around 700,000 cells was selected for the final simulations, as it strikes an optimal balance between accuracy and computational efficiency. This mesh quality was evaluated based on skewness and orthogonal quality criteria, where skewness values below 0.94 and orthogonal quality values above 0.15 were considered acceptable to ensure stable and reliable numerical simulation.

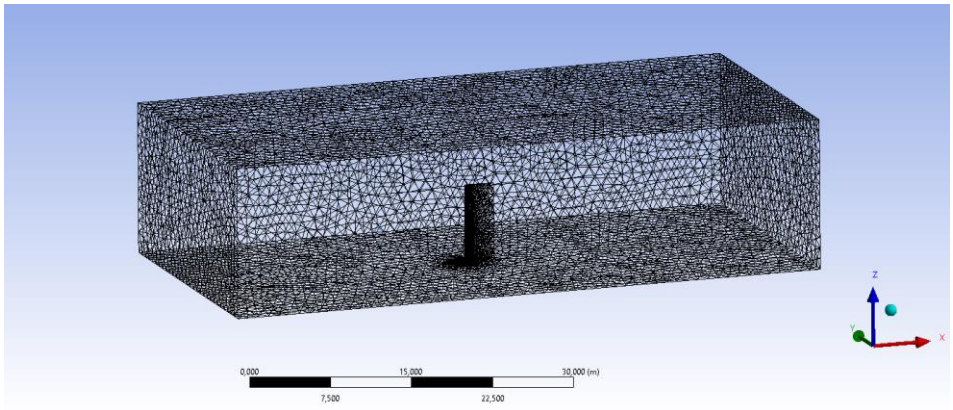

Figure 10. Mesh in configuration 1 wingsail

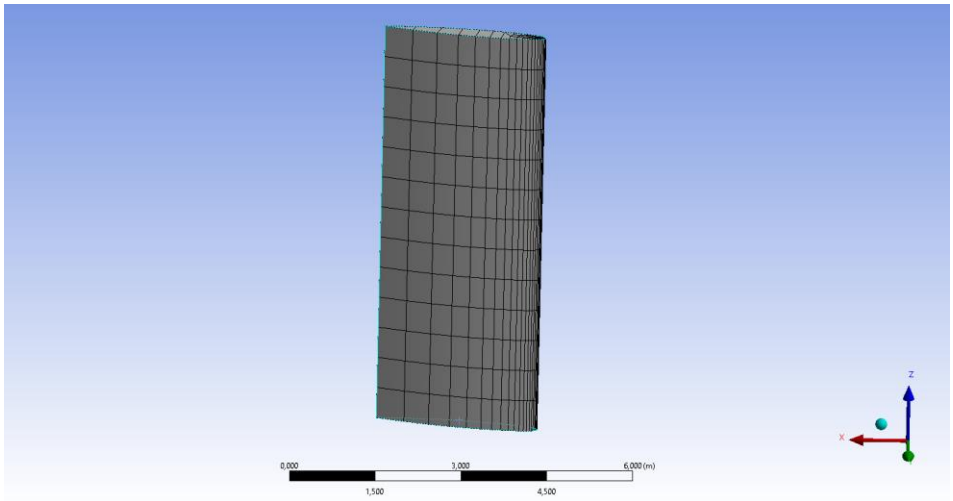

Figure 11. Mesh on the wingsail surface

The main input parameters for CFD simulations performed using ANSYS Fluent are summarized in Table 5; the simulations were conducted using a pressure-based solver to model steady external aerodynamic flow around the wingsail. These parameters include the boundary conditions, the model, and the convergence criteria, which were defined to ensure a stable numerical solution. The wind speeds considered in this study were 4 m/s, 10 m/s, 13.7 m/s, and 17.2 m/s, and the angle of attack was varied from −5°, 0°, 5°, 10°, 15°, and 20°. Additionally, two wingsail placement configurations were analyzed: a midship arrangement and a combined midship-aft arrangement. The k-ω Shear Stress Transport (SST) turbulence model was employed in this study. Compared to other turbulence models, it offers improved accuracy in predicting adverse pressure gradients and flow separation, making it well-suited for aerodynamic simulations of wingsail configurations [9]

Table 5. CFD Parameters

Input Parameter	Specification
Solver type	Pressure-based
Inlet Condition	Velocity inlet
Outlet Condition	Pressure outlet (0 Pa gauge pressure)
Wingsail Surface	No-slip wall
Top and Bottom Boundary	Symmetry
Front and Rear Boundary	Walls
Side Boundary	Inlet/Outlet
Turbulence model	k-ω Shear Stress Transport (SST)
Residual Convergence criterion	Residuals < 10^{-5}

3. Results and Discussion

Figure 13 shows that the drag coefficient varies only slightly as the number of cells increases, indicating that the solution is not highly sensitive to mesh refinement. The values begin to stabilize at around 700,000 cells, with only minor fluctuations beyond this point. From coarse to finer mesh levels, the changes remain small, suggesting that the drag prediction has already reached a stable solution even at relatively coarse meshes. Therefore, further mesh refinement has little influence on the computed drag values, indicating that the selected mesh density is sufficient to provide reliable results while maintaining computational efficiency.

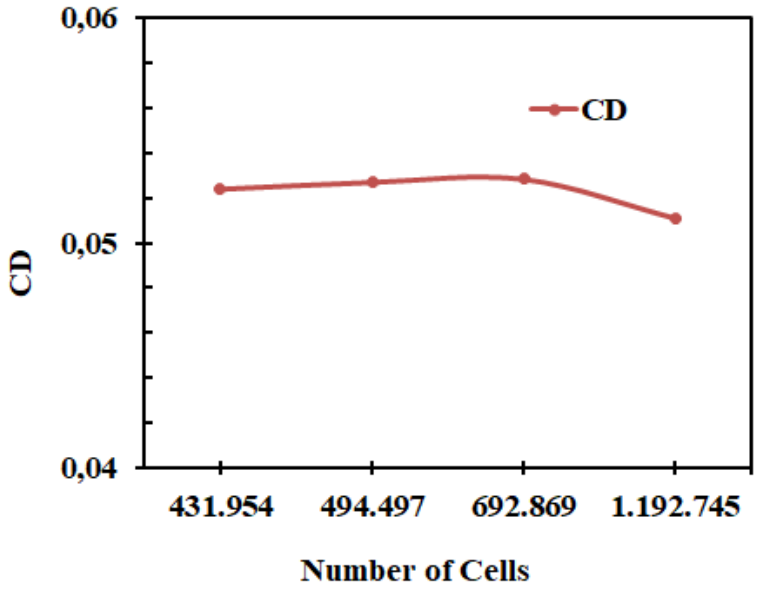

Figure 12. Grid independence test for drag coefficient

Figure 14 demonstrates that the pressure distribution in the W2 configuration becomes increasingly pronounced as the angle of attack increases. At an angle of attack (AoA) of 5°, the pressure difference between the upper and lower surfaces of the wingsail remains moderate, which indicates stable lift generation with minimal flow disturbance. At an AoA of 10°, the low-pressure region on the upper surface expands, while the high-pressure region on the lower surface becomes more distinct, resulting in greater lift enhancement. At an AoA of 20°, the high-pressure region on the lower surface intensifies significantly, accompanied by a more dispersed pressure pattern downstream of the wingsail. This pattern indicates increased flow disturbance, which contributes to higher drag, while the lift force remains substantial.

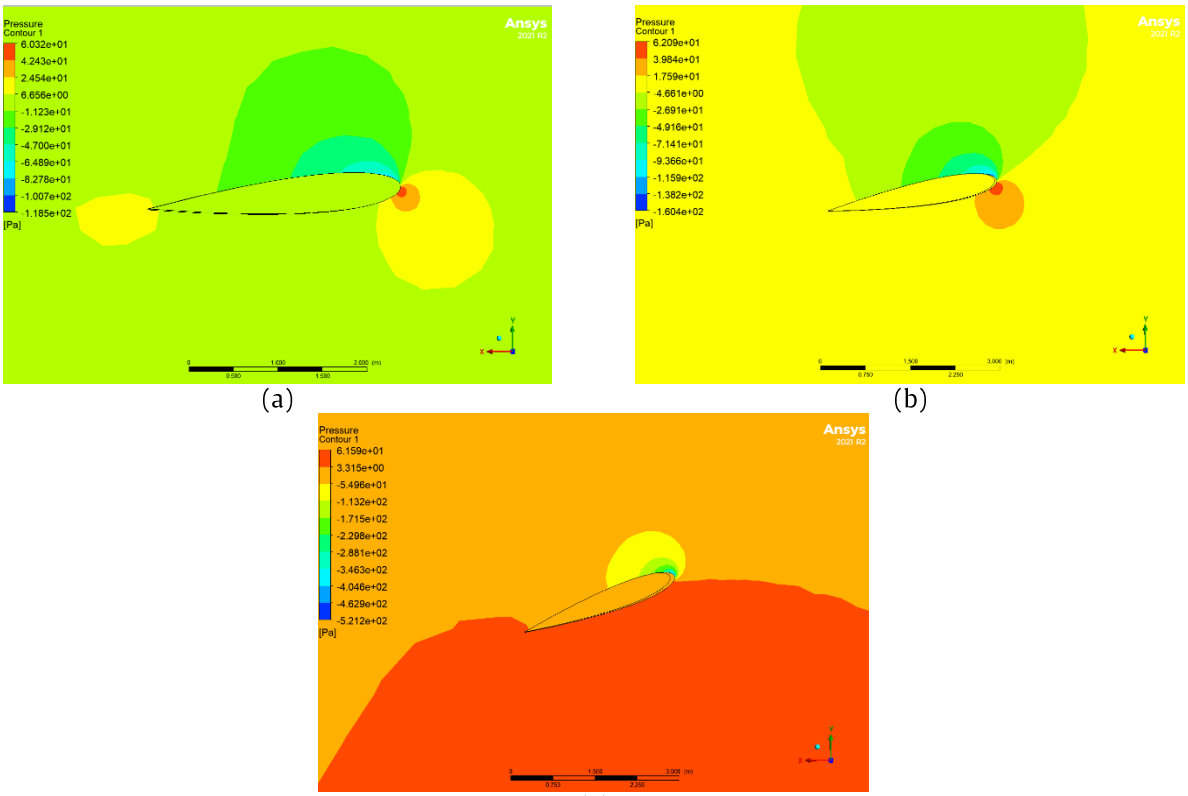

Figure 13. Pressure contour distribution of the W2 wingsail at 10 m/s for angles of attack of: (a) 5°, (b) 10°, and (c) 20°

Figure 15 shows the effect of angle of attack on the lift and drag coefficients of the W1 and W2 wingsail configurations. For both configurations, the lift coefficient increases with increasing angle of attack, rising from negative values at −5° to a maximum at 20°. This behavior is attributed to the increasing pressure difference between the upper and lower surfaces of the wingsail and is consistent with classical airfoil theory [15]. Although no clear indication of a full stall is observed, the lift coefficient approaches its maximum at higher angles of attack, suggesting the onset of flow separation. At the same angle of attack, W1 generally produces slightly higher lift values, particularly at medium to high angles, although this is accompanied by a modest increase in drag compared to W2. Overall, the highest aerodynamic efficiency occurs at moderate angles of attack (5°–10°), while W2 exhibits more stable performance at higher angles.

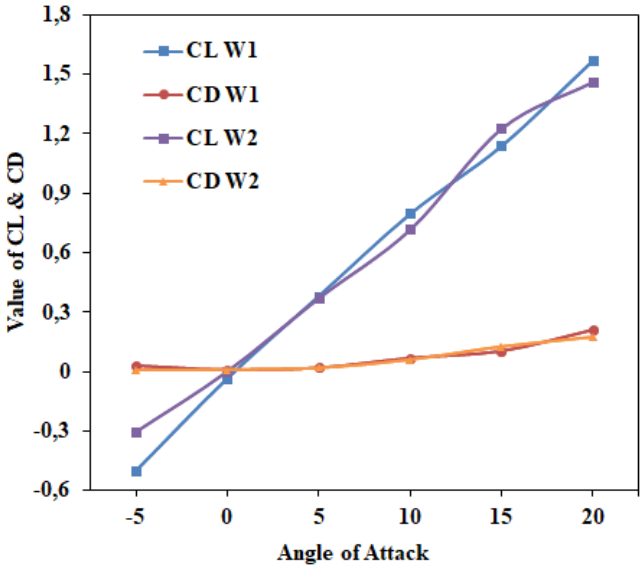

Figure 14. CL and CD characteristics of W1 and W2 at various angles of attack

Figures 16–19 illustrate the influence of wind speed on the lift and drag coefficients for wingsail configurations W1–W4 across a range of angles of attack. For all configurations, the lift coefficient increases with increasing angle of attack and reaches a maximum at 20°. At low angles of attack, wind speed has a relatively minor influence on lift, as indicated by the small differences between the curves. However, between 10° and 20°, higher wind speeds result in significantly greater lift due to increased aerodynamic forces and enhanced pressure differences around the wingsail.

Meanwhile, the drag coefficient remains low at small angles of attack but increases as the angle of attack increases, particularly at higher angles. This behavior is associated with increased pressure drag and the formation of a larger wake region behind the wingsail. Although higher wind speeds enhance lift generation, they also lead to increased drag, resulting in a less proportional improvement in aerodynamic efficiency. Based on these results, wind speeds between 10 and 13.7 m/s provide the most favorable balance between lift and drag across all configurations.

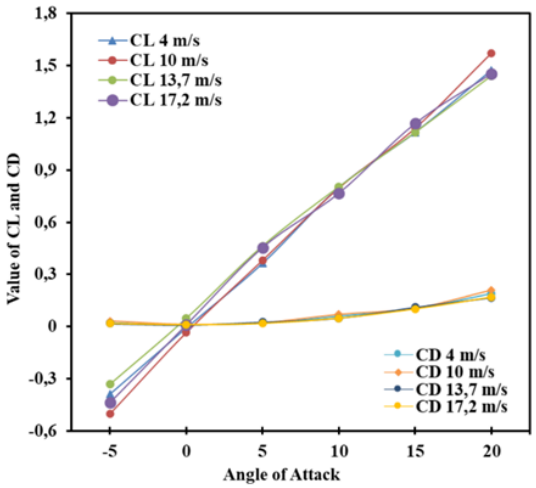

Figure 15. Effect of Wind Speed on CL and CD of W1

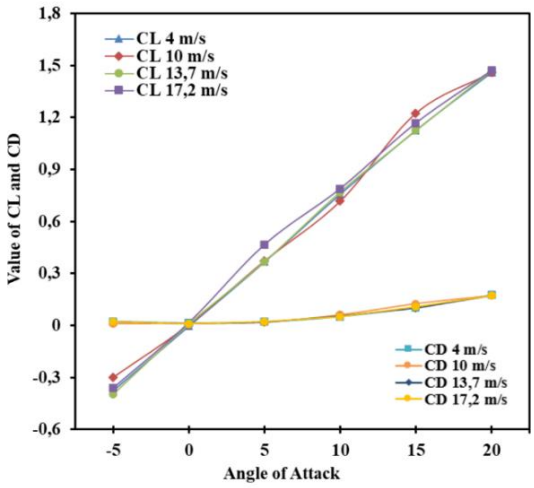

Figure 16. Effect of Wind Speed on CL and CD of W2

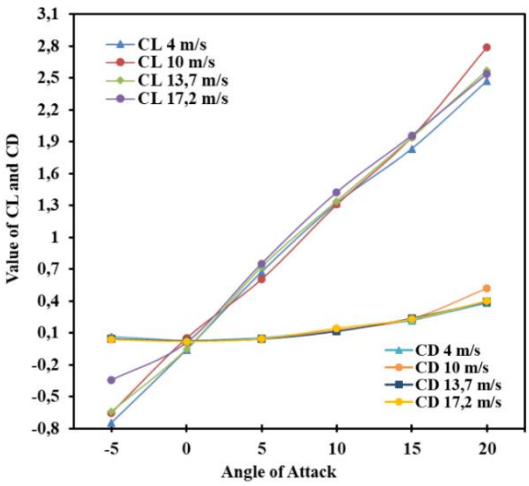

Figure 17. Effect of Wind Speed on CL and CD of W3

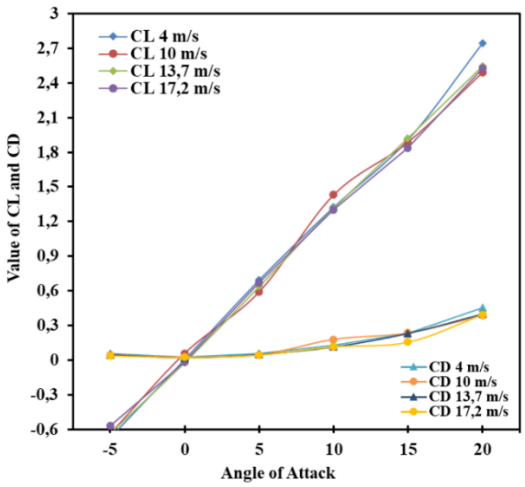

Figure 18. Effect of Wind Speed on CL and CD of W4

At an angle of attack of 5° (Figures 20 and 21), the single wingsail configurations positioned at the center of the vessel (W1 and W2) generate lower lift coefficient values than the center–rear configurations (W3 and W4). In contrast, the difference in drag coefficient remains relatively small due to the relatively stable airflow at low angles of attack. As the angle of attack increases to 10° (Figures 22 and 23), the gap in lift coefficient between W1–W2 and W3–W4 becomes more pronounced, indicating clearer aerodynamic benefits from the double wingsail arrangement despite a moderate increase in drag for W3 and W4, which is associated with enhanced aerodynamic interaction between the wingsails. At a higher angle of attack of 20° (Figures 24 and 25), W3 and W4 show the largest increase in lift compared with W1 and W2; however, this gain is accompanied by a substantial increase in drag, suggesting that drag effects become increasingly dominant due to stronger flow separation and wake interaction between the front and rear wingsails, leading to increased turbulence and energy loss. Overall, these results indicate that the influence of wingsail placement in the W3 and W4 configurations becomes more significant at higher angles of attack. At the same time, W1 and W2 exhibit more stable but less enhanced aerodynamic performance.

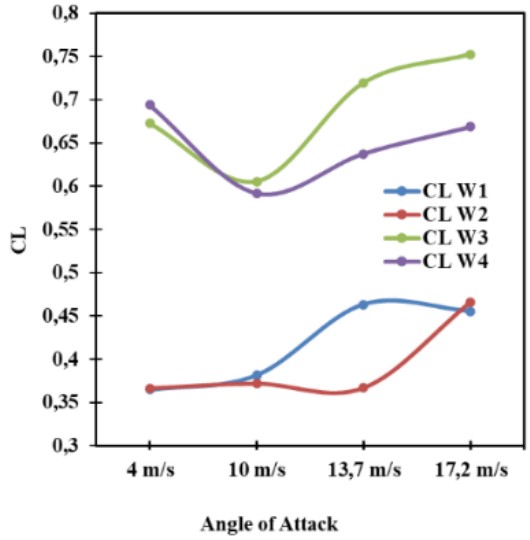

Figure 19. Effect of wingsail placement on CL at AoA 5°

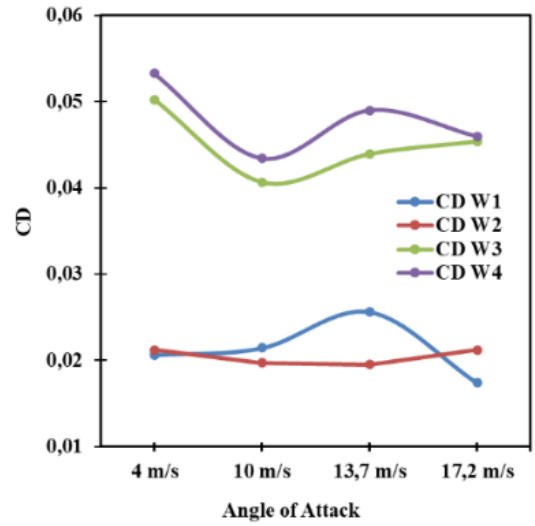

Figure 20. Effect of wingsail placement on CD at AoA 5°

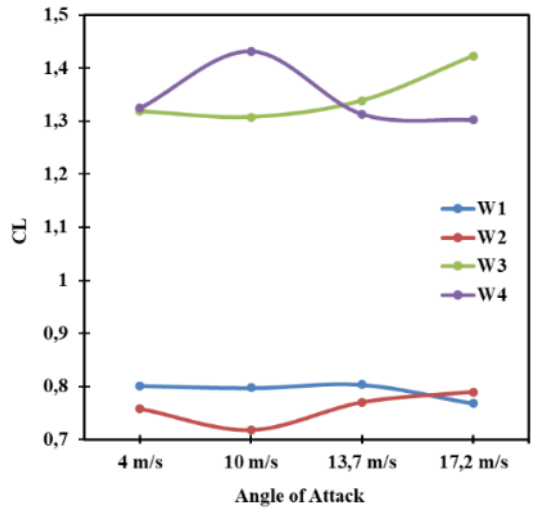

Figure 21 Effect of wingsail placement on CL at AoA 10°

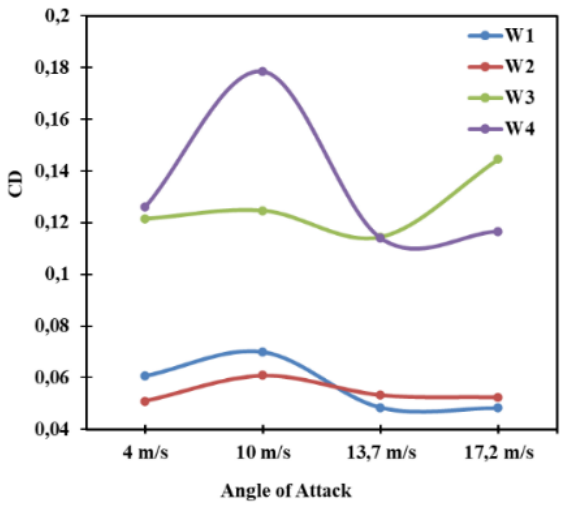

Figure 22 Effect of wingsail placement on CD at AoA 10°

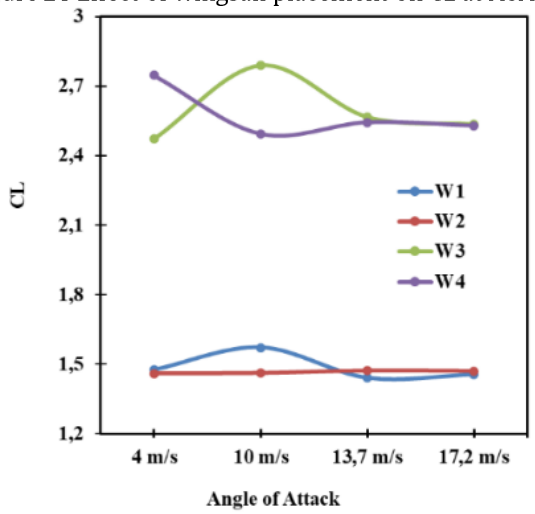

Figure 23. Effect of wingsail placement on CL at AoA 20°

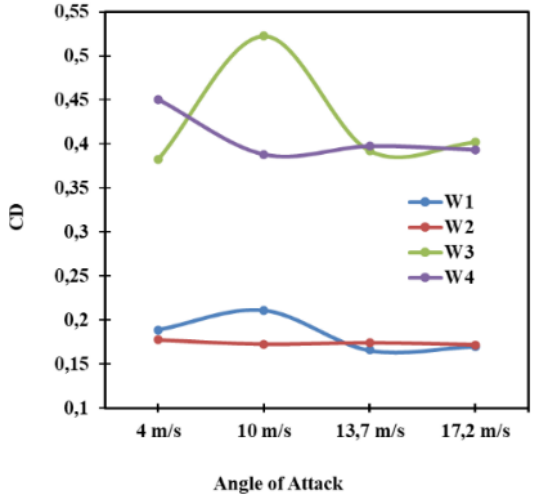

Figure 24 Effect of wingsail placement CD at AoA 20°

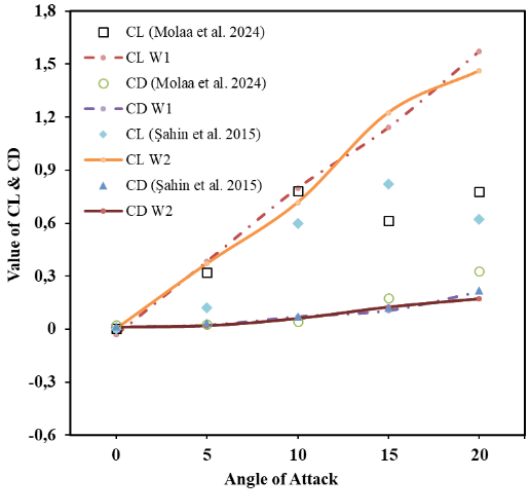

Figure 25 Comparison of CL and CD with the research of Molaa et al [23] and Şahin et al [24]

Figure 26 shows a comparison of the lift coefficient and drag coefficient obtained from CFD simulations for the W1 and W2 wingsail configurations. The validation was performed using data from the literature [23] and [24], used for CFD model validation. In the [23] dataset, several CL and CD values at specific angles of attack were obtained by extrapolating from available literature data to allow meaningful trend comparisons. The results show that the CL and CD values from the CFD simulations exhibit trends consistent with reference data. Specifically, the lift coefficient increases with increasing angle of attack, while the drag coefficient increases gradually, particularly at medium to high angles of attack. The discrepancies observed at high angles of attack remain acceptable and are likely influenced by differences in Reynolds number, numerical methods, and the turbulence models employed. Therefore, the CFD model used in this study is sufficiently valid for further analysis.

4. Conclusion

Based on the overall analysis, the W2 wingsail (NACA 0015) is recommended over the W1 configuration (NACA 0012) due to its more stable aerodynamic behavior and more controlled drag increase. Although W1 can generate slightly higher lift under certain conditions, this advantage is accompanied by higher drag. In terms of wind speed, the wingsail performs most effectively at medium wind speeds, approximately 10–13.7 m/s, where a better balance between lift and drag is achieved across all tested configurations. Configurations with wingsails positioned at both the middle and rear of the vessel (W3 and W4) consistently generate greater lift compared to single wingsail arrangements located solely in the middle (W1 and W2). However, this improvement in lift is accompanied by a corresponding increase in drag. Considering the combined influences of airfoil shape, wind speed, and wingsail placement. The W4 configuration (NACA 0015 with middle and rear placement) is identified as the most suitable option. This configuration provides an optimal balance between increased lift and aerodynamic stability, particularly at medium wind speeds typical of fishing vessel operations.

Acknowledgements

Acknowledgment is extended to the Research Center for Hydrodynamics Technology, BRIN (Badan Riset dan Inovasi Nasional), through the MBKM (Merdeka Belajar Kampus Merdeka) internship program 2025 (MBKM-BRIN-198032/VII/2025), for providing technical guidance and facilities during this study. Appreciation is also expressed to all parties who contributed to the research process.

References

[1] S. Deng and Z. Mi, "A review on carbon emissions of global shipping," Dec. 01, 2023, *Springer*. doi: https://doi.org/10.1007/s44312-023-00001-2.
[2] L. Čampara, N. Hasanspahić, and S. Vujičić, "Overview of MARPOL ANNEX VI regulations for prevention of air pollution from marine diesel engines," *SHS Web of Conferences*, vol. 58, p. 01004, 2018, doi: https://doi.org/10.1051/shsconf/20185801004.
[3] Ranqi Ma *et al.*, "Energy efficiency improvement technologies for ship in operation: A comprehensive review," *Ocean Engineering*, vol. Volume 331, Apr. 2025, doi: https://doi.org/10.1016/j.oceaneng.2025.121258.
[4] F. Thies and J. W. Ringsberg, "Sea trials vs prediction by numerical models–Uncertainties in the measurements and prediction of WASP performance," *Journal of Ocean Engineering and Science*, 2024, doi: https://doi.org/10.1016/j.joes.2024.05.001.
[5] ITTC, "Report of the Wind Powered and Wind Assisted Ships Committee," 2024.
[6] IMO, "What are rigid/hard wing sails and how do they work?" Accessed: Mar. 18, 2025. [Online]. Available: https://futurefuels.imo.org/faq/what-are-rigid-hard-wing-sails-and-how-do-they-work/
[7] D. Li, Y. Zhang, P. Li, J. Dai, and G. Li, "Aerodynamic performance of a new double-flap wing sail," *Polish Maritime Research*, vol. 26, no. 4, pp. 61–68, Dec. 2020, doi: https://doi.org/10.2478/pomr-2019-0067.

[8] M. N. Nyanya, H. B. Vu, A. Schönborn, and A. I. Ölçer, "Wind and solar assisted ship propulsion optimisation and its application to a bulk carrier," *Sustainable Energy Technologies and Assessments*, vol. 47, Oct. 2021, doi: https://doi.org/10.1016/j.seta.2021.101397.
[9] M. Daluar Hussain and O. Md Amin, "A Comprehensive Analysis of the Stability and Powering Performances of a Hard Sail-Assisted Bulk Carrier," *Journal of Marine Science and Application*, 2021, doi: https://doi.org/10.1007/s11804-021-00219-w.
[10] A. Akbar, "Effect of Angle of Attack on Airfoil NACA 0012 Performance," *Rekayasa Energi Manufaktur Jurnal*, vol. 5, no. 1, pp. 2528–3723, 2020, https://rem.umsida.ac.id/index.php/rem/article/view/1235.
[11] M. F. Hidayat, "Analisa aerodinamika airfoil NACA 0012 dengan ANSYS Fluent," *Jurnal Kajian Teknologi*, vol. 10, no. 2, pp. 73–83, 2014. https://journal.untar.ac.id/index.php/teknologi/article/view/250.
[12] A. Mula and M. Abdulwahid, "Numerical Simulation of the Aerodynamic Characteristics of NACA0012 Airfoil Based on Operational Parameters," *Basrah journal for engineering science*, vol. 23, no. 1, pp. 81–89, Jul. 2023.
[13] C. J. von Klemperer, R. A. D. Horwitz, and A. G. Malan, "An articulating wingsail design for Wind Assisted Ship Propulsion (WASP) applications," *Sci. Afr.*, vol. 20, Jul. 2023, doi: https://doi.org/10.1016/j.sciaf.2023.e01699.
[14] P. Dian, M. R. Utina, Rina, S. Endah, and S. Nanang, "Model Experiment on Fishing Vessel Operation in Benoa, Bali, Using Wind-Assisted Propulsion System," Research Report PRTH-BRIN Surabaya, Indonesia, 2025.
[15] S. Fang *et al.*, "Aerodynamic Analysis of Rigid Wing Sail Based on CFD Simulation for the Design of High-Performance Unmanned Sailboats," *Mathematics*, vol. 12, no. 16, Aug. 2024, doi: https://doi.org/10.3390/math12162481.
[16] H. Zhu, H. D. Yao, F. Thies, J. W. Ringsberg, and B. Ramne, "Propulsive performance of a rigid wingsail with crescent-shaped profiles," *Ocean Engineering*, vol. 285, Oct. 2023, doi: https://doi.org/10.1016/j.oceaneng.2023.115349.
[17] C. Li, H. Wang, and P. Sun, "Study on the Influence of Gradient Wind on the Aerodynamic Characteristics of a Two-Element Wingsail for Ship-Assisted Propulsion," *Journal of Marine Science and Engineering*, vol. 11, no. 1, Jan. 2023, doi: https://doi.org/10.3390/jmse11010134.
[18] T. E. Makram, P. Panagiotou, and D. Mattheou, "Wingsail layout design and shape optimization using a CFD-aided Taguchi approach: The Aegean Marathon case study," *Ocean Engineering*, vol. 276, May 2023, doi: https://doi.org/10.1016/j.oceaneng.2023.114055.
[19] DNV, "Wind Assisted Propulsion Systems," DNV. Accessed: Apr. 08, 2025. [Online]. Available: https://www.dnv.com/maritime/insights/topics/waps-wind-assisted-propulsion-systems/
[20] M. H. Khalid, "CFD Analysis of NACA 0012 Aerofoil to Investigate the Effect of Increasing Angle of Attack on Coefficient of Lift and Coefficient of Drag," *Journal of Studies in Science and Engineering*, vol. 2, no. 1, pp. 74–86, Mar. 2022, doi: https://doi.org/10.53898/josse2022216.
[21] "Airfoil Tools." Accessed: Jun. 24, 2025. [Online]. Available: Airfoil Tools
[22] Cristina Aleixendri, "bound4blue installs its eSAIL system on the fishing vessel 'Balueiro Segundo.' " Accessed: Apr. 18, 2026. [Online]. Available: https://bound4blue.com/bound4blue-installs-its-esail-system-on-the-fishing-vessel-balueiro-segundo/
[23] A. A. Molaa and M. A. Abdulwahid, "Numerical and experimental study of the impact on aerodynamic characteristics of the NACA0012 airfoil," *Open Engineering*, vol. 14, no. 1, Jan. 2024, doi: https://doi.org/10.1515/eng-2022-0506.
[24] i. Şahin and A. Acir, "Numerical and Experimental Investigations of Lift and Drag Performances of NACA 0015 Wind Turbine Airfoil," *International Journal of Materials, Mechanics and Manufacturing*, vol. 3, no. 1, pp. 22–25, 2015, doi: https://doi.org/10.7763/ijmmm.2015.v3.159.